Experimental Studies of Contact Detachment Delay in Microrelays for Logic Applications

Yenhao Chen, I-Ru Chen, Chuang Qian, Alexis Peschot, and Tsu-Jae King Liu, *Fellow, IEEE*

***Abstract*— The abrupt switching behavior of mechanical switches makes it imperative to ensure that they turn OFF more rapidly than they turn ON. In a complementary logic circuit, slower turn-OFF than turn-ON could lead to the formation of a direct current path between the power supply and the ground, which would result in undesirable dynamic power dissipation during signal transitions. In this brief, the contact detachment delay (τ_{CD}) of microrelays is systematically characterized and investigated. τ_{CD} is shown to be correlated with contact adhesive force and the mechanical properties of the contact materials; τ_{CD} can also be reduced by ultrathin-oxide coating and contact area scaling.**

***Index Terms*— Contact detachment delay, crowbar current, microrelay, pull-in delay, reliability.**

I. Introduction

ADVANCEMENTS in CMOS technology over the past few decades have led to tremendous improvements in integrated-circuit operating speed and cost per function as well as increased chip functionality, stemming from increased transistor density. But the semiconductor industry is now struggling with a chip power density crisis due to the nonscalability of the thermal voltage (k_BT/q), which sets the minimum subthreshold swing of a MOSFET and hence limits reductions in transistor threshold voltage. In contrast to electronic switches, mechanical switches operate by making/breaking physical contact and therefore offer the ideal characteristics of zero OFF-state leakage current and abrupt transition between ON/OFF states, which provide for zero static power dissipation and (in principle) very low switching voltage, respectively. Therefore, microrelay technology has attracted interest for digital integrated-circuit application in recent years [1]. It has been projected that a scaled relay technology can provide for more than 10× improvement in energy efficiency compared with CMOS technology at the same node [2].

Ideally, the operating speed of a relay-based integrated circuit is limited by the mechanical switching time rather than the electrical delay (charging/discharging time) [2].

Manuscript received June 20, 2014; revised March 21, 2015, May 21, 2015, and June 15, 2015; accepted June 16, 2015. Date of current version July 21, 2015. This work was supported by the National Science Foundation under Award 0939514. The review of this brief was arranged by Editor F. Ayazi. *(Corresponding author: Yenhao Chen.)*

Y. Chen, C. Qian, A. Peschot, and T.-J. K. Liu are with the Department of Electrical Engineering and Computer Sciences, University of California at Berkeley, Berkeley, CA 94720 USA (e-mail: ychen@eecs.berkeley.edu; cqian@eecs.berkeley.edu; peschota@berkeley.edu; tking@eecs.berkeley.edu).

I.-R. Chen is with Xilinx Inc., San Jose, CA 95124 USA (e-mail: iruchen@eecs.berkeley.edu).

Color versions of one or more of the figures in this paper are available online at http://ieeexplore.ieee.org.

Digital Object Identifier 10.1109/TED.2015.2446960

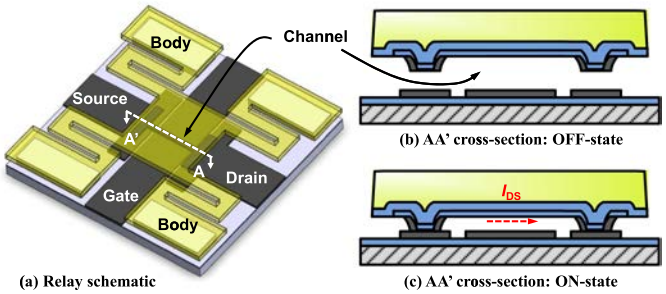

Fig. 1. Schematic of the 4T logic relay used in this brief. (a) Plan view illustrating the various terminals. (b) Cross-sectional view along $A - A'$ in the OFF state and (c) in the ON state.

Previous studies of mechanical switching time have focused on turn-ON delay, specifically pull-in dynamics [3] and methods for reducing the pull-in voltage (V_{PI}) and pull-in delay (τ_{PI}) [4]. Since very large contact resistance ($R_{ON} > 10$ kΩ) can significantly reduce computational throughput, R_{ON} stability has also been investigated extensively for various contact materials and relay operating conditions [5], [6].

In contrast, the turn-OFF delay of microrelays was reported but has not yet been studied in detail [7]. This is because it is generally assumed that a relay turns OFF more quickly than it turns ON, since a relatively small separation (∼1 nm) between the contacting electrodes is sufficient to prevent current flow, i.e., the mechanical displacement required to turn OFF a relay is smaller than that required to turn ON a relay. However, the time required to break physical contact (before the contacting electrodes can move apart) can be significant due to surface adhesion [8]. If the contact detachment delay (τ_{CD}) is greater than the pull-in delay τ_{PI}, then a direct current path (short circuit) between the power supply and ground can be temporarily formed in a conventional complementary logic circuit comprising at least one pull-up device connected between the output node and power supply and at least one pull-down device connected between the output node and ground; the resultant crowbar current gives rise to undesirable dynamic power dissipation [9]. In this brief, the impact of contacting electrode material, microrelay operating conditions, and device structural dimensions on τ_{CD} is systematically characterized. The impact of dimensional scaling is also investigated to provide insight for device miniaturization.

II. Relay Design and Fabrication

Fig. 1 presents the structure and operation of the four-terminal (4T) relay design for digital logic

applications [10]. When a sufficiently large voltage is applied between the movable body electrode and the underlying gate electrode (i.e., $|V_{GB}| \geq |V_{PI}|$), the body is actuated downward sufficiently to bring the channel (a metallic strip attached to the underside of the body via an intermediary insulating layer) into contact with the source and drain electrodes (which are coplanar with the gate electrode) so that current can flow ($|I_{DS}| > 0$), and hence, the relay is ON. When $|V_{GB}|$ is lowered back down to below the release voltage ($|V_{RL}|$), the spring-restoring force of the folded-flexure suspension beams overcomes the attractive (electrostatic and adhesive) forces to actuate the body upward, bringing the channel out of contact with the source/drain electrodes so that no current can flow; hence, the relay is OFF.

A four-mask process was used to fabricate the microrelays as follows. First, an insulating layer of 80-nm-thick aluminum oxide (Al_2O_3) was deposited by atomic-layer-deposition (ALD) onto the silicon wafer substrate. Then, a 70-nm-thick metal electrode layer was sputtered onto the insulated substrate. Three different contacting electrode (i.e., source/drain and channel) materials were investigated in this brief: tungsten (W), ruthenium (Ru), and nickel (Ni). W and Ru were patterned by dry etching [11], whereas Ni was patterned using a liftoff process, using the first mask. Afterward, a first sacrificial layer of low-temperature oxide (LTO) layer was deposited by low-pressure chemical vapor deposition (LPCVD) at 400 °C. The source and drain contact regions (1 μm^2 in area each, unless otherwise noted) were then defined by removing the LTO in these regions using a masked CF_4-based reactive ion etch (RIE). Subsequently, a second sacrificial layer of LTO was deposited. Its thickness (80 nm) defines the nominal contact gap thickness, whereas the total thickness of the two LTO layers (160 nm) defines the nominal actuation gap thickness. The channel (of the same material as the source and drain electrodes) was then formed by sputter deposition and patterning. (Note that the channel is dimpled in the contact regions.) After deposition of a 55-nm-thick Al_2O_3 insulating layer, a structural layer of *in situ* boron-doped polycrystalline silicon-germanium (poly-$Si_{0.35}Ge_{0.65}$) was deposited by LPCVD and patterned by HBr/Cl_2-based RIE. Finally, the sacrificial LTO layers were selectively removed in hydrogen fluoride (HF) vapor to release the structure. Some relays with W electrodes were coated after release with an ultrathin layer of TiO_2 by ALD.

III. Test Setup

The fabricated microrelays are transferred to a Lakeshore TTPX vacuum probe station for characterizations soon after HF vapor release, to minimize contact surface contamination. In this sealed vacuum chamber (accompanied with a Varian V-81 turbo pump and a dry scroll pump), the temperature, pressure, and relative humidity are kept at 300 K, ~5 μtorr, and ~0%, respectively. In general, the devices exhibit relatively high R_{ON} (~10 kΩ) for the first switching cycle and hence are subjected to a high-voltage ($V_{DS} \sim 6$ V along with current compliance) burn-in process [12] using the HP4155B semiconductor parameter analyzer to reduce R_{ON} to below 0.9 kΩ, depending on the contact material. The contact

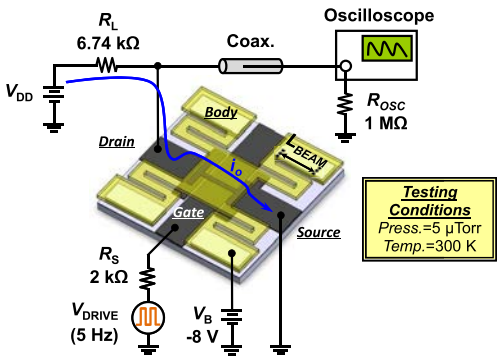

Fig. 2. Schematic of the resistive-load inverter test setup.

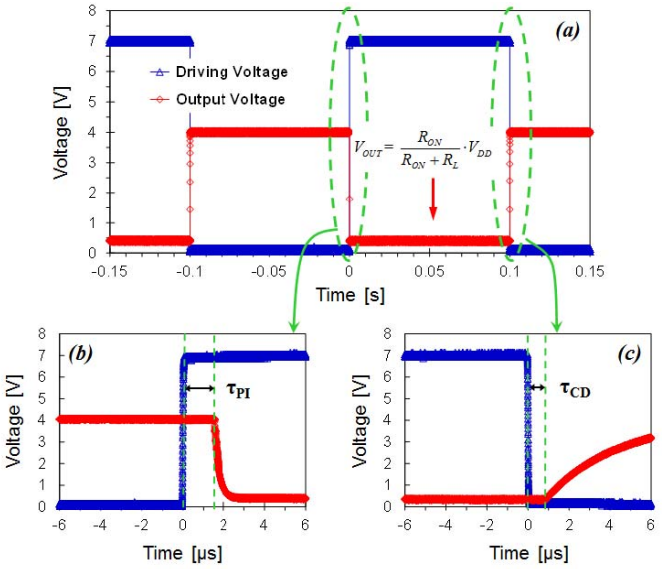

Fig. 3. (a) Measured input and output voltage waveforms for the setup in Fig. 2 (with $V_D = 4$ V, $V_{DRIVE} = 7$ V, and $V_B = -8$ V), with zoomed-in views of the regions of (b) relay turn-ON and (c) relay turn-OFF.

detachment delay measurements are performed after the burn-in procedure. Without the process, the residual contamination layer such as hydrocarbons [13] and some metal oxides [14] (which have lower surface energy compared with the metal counterparts) could alter the adhesion force and subsequently τ_{CD} [13]. It should be noted that minute amounts of oxygen and contaminants (such as hydrocarbons) can cause thin insulating films to form at the contacting asperities over time, especially during the course of many hot-switching cycles.

Relay switching delays are monitored using a resistive-load inverter setup, as depicted in Fig. 2; the relay serves as the pull-down device and a resistor serves as the pull-up device. The cyclic evolution of ON-state resistance (R_{ON}) [14], as well as τ_{PI} and τ_{CD}, is monitored, as shown in Fig. 3. When the relay is ON, a direct current path exists between the power supply (V_{DD}) and ground, and the output voltage is given by the voltage divider formula shown in Fig. 3(a). τ_{PI} is defined as the difference between the time that $|V_{GB}|$ increases above $0.5|V_{DRIVE}|$ and the time that the output voltage begins to fall toward ground, as shown in Fig. 3(b). τ_{CD} is defined

TABLE I
MECHANICAL PROPERTIES OF CONTACT MATERIALS

Materials	TiO_2	W	Ru	Ni
Surface energy, γ (J/m^2)	0.89 [19]	3.675 [20]	3.050 [20]	2.450 [20]
Young's modulus, E (GPa) [21]	--	360	430	216
Poisson ratio, ν [21]	--	0.28	0.30	0.31
Estimated hardness, H (GPa)	--	21.3 [22]	15.28 [23]	6 [24]
Normalized adherence force	0.24	1	1.65	2.73

as the difference between the time that $|V_{GB}|$ falls below $0.5|V_{DRIVE}|$ and the time that the output voltage begins to rise toward V_{DD}, as depicted in Fig. 3(c). This is essentially the time it takes for the channel/dimples to be fully detached from the bottom source/drain electrodes after the relay driving voltage is removed.

The body (structure) is biased at -8 V to lower the gate voltage required to switch the relay, to <3 V. The hysteresis voltage V_H sets the lower limit for relay V_{PI} and restricts the maximum body bias that can be applied; this allows V_{DRIVE} to be scaled down to 3 V (further increase in $|V_B|$ will cause the device to stick down when V_{RL} drops below 0 V). The maximum value of V_{DD} used in this brief is 7 V, because contact welding becomes an issue for $V_{DD} > 7$ V.

Herein, τ_{PI} and τ_{CD} are characterized for microrelays with Ni, Ru, W, and TiO_2-coated W contacting electrodes. The mechanical properties of these materials are summarized in Table I.

IV. RESULTS AND DISCUSSION

The source/drain electrode surface roughness was measured by atomic force microscopy to be approximately 0.7 nm (rms) for each of the different metals. On the other hand, the channel (top electrode) surface should be much smoother, due to conformal deposition of the relatively thick sacrificial LTO layers. A contact model between two nominally flat surfaces (with one smooth and the other rough) was developed in [15], which links the load to the summit level distribution of multiple asperities. However, actual asperity height distribution is not easily obtained and modeled, and it could vary from device to device. For simplicity, the contacting asperities are assumed to be of the same height and equally loaded, as in [16].

Furthermore, due to the nature of small loading, contacts in microsystems are typically made only between a few contacting asperities, and the number of contact points N is in the low single-digit range which can be close to zero [16]. For the purpose of providing insight into the dependences of the contact adhesive force and τ_{CD} on the contacting electrode material, N is approximated to be 1 and the contact geometry is approximated as a single hemispherical asperity compressed against a flat surface, reducing the case to sphere on flat.

Based on the analytical adhesion model summarized in [17], the adherence force (or the pull-off force) that is required to separate the contacting surfaces (sphere on flat) is described by

$$F_{adh} = \alpha\pi R\Delta\gamma. \tag{1}$$

where $\Delta\gamma\ (\equiv \gamma_1 + \gamma_2 - \gamma_{12})$ is the Dupré energy of adhesion, R is the spherical radius of the contacting asperity, and the coefficient α varies from 3/2 to 2 depending on the model of elastic contact.

It is assumed that the contact is elastic but the contact interface is maintained in a state of initial plastic deformation; such deformation determines the contact area and the adhesion force. After removal of the external load and during contact detachment, the deformed spherical surface recovers, with an effective radius of curvature R_f (considering the originally flat surface now exhibits a spherically deformed morphology), which can be derived by approximating the pressure distribution to a Hertzian contact as in [17] and [18]

$$R_f = \frac{4}{3}\frac{a_f E^*}{\pi p_m}. \tag{2}$$

where a_f denotes the radius of contact during unloading and E^* is the biaxial Young's modulus given by $E/(1-\nu^2)$ in which E is the Young's modulus and ν is the Poisson ratio. The mean pressure p_m equals to the hardness H of the material when the entire contact undergoes plastic deformation. Consider the contact junction itself to have a circular shape with radius a_f, and the effective radius is related to contact force by

$$a_f = \sqrt{\frac{F_{load}}{\pi p_m}}. \tag{3}$$

Combining (2) and (3), (1) reduces to

$$F_{adh} = \alpha\pi R_f\Delta\gamma = \frac{4\alpha\Delta\gamma E^* F_{load}^{\frac{1}{2}}}{3(\pi p_m^3)^{\frac{1}{2}}} \tag{4}$$

as given in [17] and [18].

The switching delays of the fabricated microrelays are compared herein for the same operating voltage conditions and hence the same F_{load}. Since the adhesion energy $\Delta\gamma$ is the sum of the surface energies γ_1 and γ_2 minus the interfacial energy γ_{12} (which equals to 0 when the two contacting surfaces are composed of identical material), the term reduces to $2\gamma_1 (= 2\gamma_2)$. As a result, any difference in adherence force is due to differences in the contact material mechanical properties

$$F_{adh} \propto \frac{\gamma E^*}{H^{3/2}}. \tag{5}$$

Therefore, the ratio of surface energy times the effective Young's modulus to hardness should be positively correlated to adhesion, i.e., higher $\gamma E^*/H^{3/2}$ should correspond to higher F_{adh}. The relative values of adhesion force listed in Table I for the contact materials studied in this brief are normalized to the value for W, using (5). For TiO_2-coated W electrode, the Young's modulus and the hardness are assumed to be the same as for W, since the volume of the ultrathin ALD coating is very small relative to that of the W electrode; it mainly alters the surface energy. The surface energies of the contact metals after the burn-in

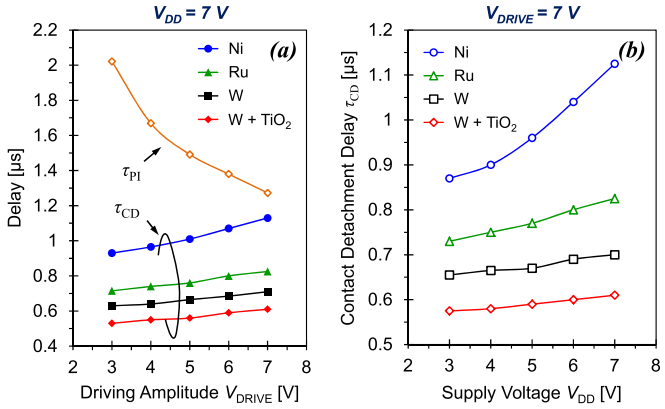

Fig. 4. Contact detachment delay (τ_{CD}) and pull-in delay (τ_{PI}) of microrelays with different contact electrode materials (a) versus actuation voltage (V_{DD} = 7 V) and (b) versus supply voltage (V_{DRIVE} = 7 V). $L_{BEAM} = 15$ μm.

process are assumed to be the same as those reported in [20] and listed in Table I. It should be noted that the hardness of a thin-film material usually is higher than that of a bulk material due to grain-boundary strengthening; this is known as the Hall–Petch effect. In [22]–[24], the microhardness of sputtered thin films (comparable in thickness to the electrode layer in this brief) was determined directly by nanoindentation tests. The values in Table I are extracted from [22]–[24] at an indentation depth of 70 nm.

Fig. 4 compares the average measured values of τ_{CD} for microrelays employing different contact materials, as a function of the supply voltage V_{DD}. (Ten devices were measured for each of contact type; the standard deviation σ for τ_{PI} is 0.1 μs, and σ for τ_{CD} is 0.03 μs.) These devices have very similar values of τ_{PI}, since their poly-$Si_{0.35}Ge_{0.65}$ structures are identical in design. The measured trend of τ_{CD} for different contact materials is as expected, since $F_{adh,Ni} > F_{adh,Ru} > F_{adh,W} > F_{adh,TiO2/W}$ (see Table I).

From Fig. 4(a), it can be seen that τ_{CD} increases with the amplitude of the driving voltage. An increase in gate actuation voltage enhances the contact force due to quadratic growth in electrostatic attraction. As the external load rises, a_f (which can be interpreted as an equivalent contact radius as if only one spot were in contact) widens according to (3). In any case, the real contact area increases with increasing contact force, leading to larger adhesive force and hence longer τ_{CD}. The rate of change in F_{adh} to F_{load} is also proportional to the factor $\gamma E^*/H^{3/2}$, which can be shown by differentiating (4) with respect to F_{load}. Thus, contact electrodes exhibiting higher initial values of τ_{CD} would respond to the change in F_{load} more rapidly, as seen in the Ni electrodes.

Fig. 4(b) shows that τ_{CD} increases with the supply voltage V_{DD}. A possible explanation for this trend is an increase in real contact area with increasing V_{DD} due to increased power dissipation (joule heating). The steady-state temperature T_m at a contact spot, given a contact voltage V_C across the junction, can be estimated using the Kohlrausch-relation as in [25]

$$T_m = T_0 + \frac{V_C^2}{8\lambda\rho} \tag{6}$$

TABLE II
THERMAL/ELECTRICAL PROPERTIES OF CONTACT MATERIALS

Materials	W	Ru	Ni
Thermal coductivity @ 20°C, λ (W·m^{-1}·k^{-1}) [21]	167	105	92
Electrical resistivity @ 20°C, ρ (μΩ·cm)	~24	~22	~18
R_{ON} @ V_{DD} = 7 V (Ω)	~700	~480	~250
V_C @ V_{DD} = 7 V (V)	~0.284	~0.190	~0.089
Estimated temperaure at contact spot @ V_{DD} = 7 V, T_m (°C)	272	215	80
Softening temperature (°C) [21]	1000	430	520

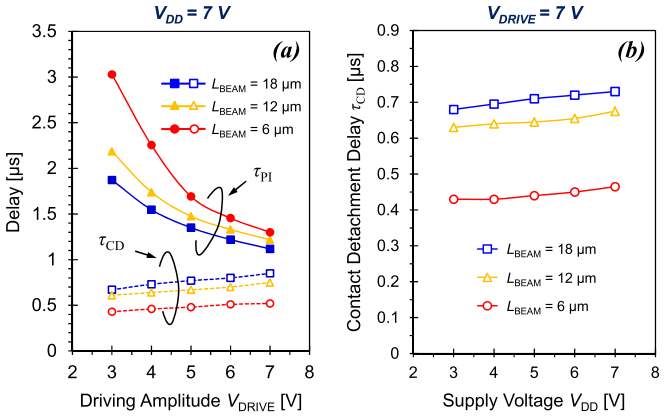

Fig. 5. Contact detachment delay (τ_{CD}) and pull-in delay (τ_{PI}) of W microrelays with different suspension beam length (L_{BEAM}) (a) versus actuation voltage (V_{DD} = 7 V) and (b) versus supply voltage (V_{DRIVE} = 7 V).

where T_0 is the temperature far away from the contact spot (assumed to be 20 °C), λ is the thermal conductivity [21], and ρ is the electrical resistivity (calculated by multiplying the measured sheet resistance by the film thickness) of the material. Note that to estimate the de-embedded V_C (across a single contact) one must take into account the trace resistance R_{trace} (comprising ~28 squares) from the source/drain signal paths. The true contact resistance R_C for each single contact is given by $(R_{ON} - R_{trace})/2$ and V_C can be calculated as

$$V_C = \frac{R_C}{2R_C + R_{trace} + R_L} V_{DD}. \tag{7}$$

Calculations predict that the temperature exceeds 80 °C for high V_{DD} but is still well below the softening temperature (see Table II), for each of the contact materials. However, it has been experimentally shown that the melting temperature of small particles can be lower than that of bulk material [26]. Therefore, softening might occur locally at some smaller contacting asperities, leading to increased contact area and τ_{CD}.

Another possible explanation for the increase of τ_{CD} with increasing V_{DD} is the removal or electrical breakdown of insulating material (native oxide, or surface contaminants) to temporarily reestablish interfacial metal-to-metal bonds at the contacting asperities [12]. Since metal-to-metal bonds having higher binding energies, the adhesion force rises consequently. We believe this is more likely to be the dominant factor to cause τ_{CD} to increase.

In addition to the contact material properties and relay operating conditions, relay design parameters also affect τ_{CD}. The stored elastic energy in the flexure beams and the

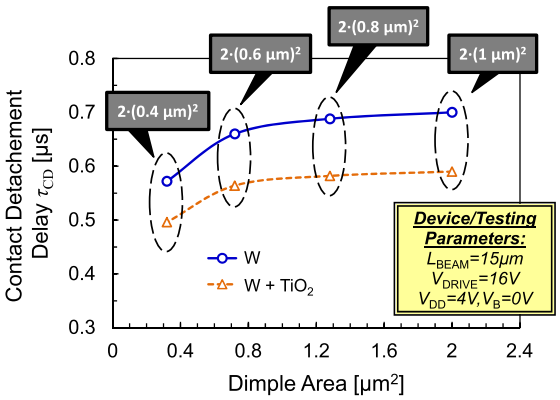

Fig. 6. Measured τ_{CD} of *W* microrelays as a function of total contact dimple area (two square dimples for each relay).

spring restoring force (which pulls the relay out of contact, to turn it OFF) is proportional to the effective spring constant (k_{eff}) of the folded-flexure suspension beams. A shorter flexure beam length introduces larger spring restoring force so that the electrodes can be separated more quickly upon removal of the hold-down force, with a tradeoff of increased V_{PI} and hence increased τ_{PI} for the same operating voltage conditions (Fig. 5). Furthermore, smaller contact dimple area is also beneficial for reducing contact adhesive force [8]. By reducing the contact dimple width from 1 to 0.4 μm, τ_{CD} is reduced from 0.7 to 0.57 μs, as presented in Fig. 6. It is observed that τ_{CD} does not scale linearly with the apparent contact area; a result reminiscent of the findings on nonlinear reduction in surface adhesive force in [27].

V. Conclusion

The contact detachment delay (τ_{CD}) of a microrelay can vary significantly with the contact electrode material, as well as relay design parameters and operating conditions. Low $\gamma\, E^*/H^{3/2}$ ratio is a favorable electrode property for reducing contact adhesive force, which also can be reduced by thin dielectric coating and scaling down the area of the contacting regions. Structural design optimization involves a tradeoff between improving turn-ON delay (τ_{PI}) and degrading turn-OFF delay; fortunately, a large design window exists for ensuring that ($\tau_{\text{PI}} > \tau_{\text{CD}}$) to avoid crowbar current in a relay-based complementary logic circuit. Selection of the operating voltage (V_{DD}) involves the same tradeoff.

References

[1] M. Spencer *et al.*, "Demonstration of integrated micro-electro-mechanical relay circuits for VLSI applications," *IEEE J. Solid-State Circuits*, vol. 46, no. 1, pp. 308–320, Jan. 2011.

[2] F. Chen, H. Kam, D. Markovic, T.-J. K. Liu, V. Stojanovic, and E. Alon, "Integrated circuit design with NEM relays," in *Proc. IEEE/ACM Int. Conf. Comput.-Aided Design*, Nov. 2008, pp. 750–757.

[3] R. K. Gupta and S. D. Senturia, "Pull-in time dynamics as a measure of absolute pressure," in *Proc. 10th Annu. IEEE Int. MEMS Workshop*, Nagoya, Japan, Jan. 1997, pp. 290–294.

[4] D. Peroulis, S. P. Pacheco, K. Sarabandi, and L. P. B. Katehi, "Electromechanical considerations in developing low-voltage RF MEMS switches," *IEEE Trans. Microw. Theory Techn.*, vol. 51, no. 1, pp. 259–270, Jan. 2003.

[5] Q. Ma *et al.*, "Metal contact reliability of RF MEMS switches," in *Proc. SPIE*, vol. 6463. 2007, pp. 646305-1–646305-13.

[6] M. P. de Boer, D. A. Czaplewski, M. S. Baker, S. L. Wolfley, and J. A. Ohlhausen, "Design, fabrication, performance and reliability of Pt- and RuO_2-coated microrelays tested in ultra-high purity gas environments," *J. Micromech. Microeng.*, vol. 22, no. 10, pp. 105027-1–105027-15, Oct. 2012.

[7] C. L. Ayala *et al.*, "A 6.7 MHz nanoelectromechanical ring oscillator using curved cantilever switches coated with amorphous carbon," in *Proc. 44th Eur. Solid State Device Res. Conf. (ESSDERC)*, Sep. 2014, pp. 66–69.

[8] B. D. Jensen, K. Huang, L. L.-W. Chow, and K. Kurabayashi, "Adhesion effects on contact opening dynamics in micromachined switches," *J. Appl. Phys.*, vol. 97, no. 10, p. 103535, May 2005.

[9] H. J. M. Veendrick, "Short-circuit dissipation of static CMOS circuitry and its impact on the design of buffer circuits," *IEEE J. Solid-State Circuits*, vol. 19, no. 4, pp. 468–473, Aug. 1984.

[10] R. Nathanael, V. Pott, H. Kam, J. Jeon, and T.-J. K. Liu, "4-terminal relay technology for complementary logic," in *IEDM Tech. Dig.*, Dec. 2009, pp. 1–4.

[11] I.-R. Chen, Y. Chen, L. Hutin, V. Pott, R. Nathanael, and T.-J. K. Liu, "Stable ruthenium-contact relay technology for low-power logic," in *Proc. 17th Int. Conf. Solid-State Sens., Actuators Microsyst. (TRANSDUCERS)*, Barcelona, Spain, Jun. 2013, pp. 896–899.

[12] B. D. Jensen, L. L.-W. Chow, K. Huang, K. Saitou, J. L. Volakis, and K. Kurabayashi, "Effect of nanoscale heating on electrical transport in RF MEMS switch contacts," *J. Microelectromech. Syst.*, vol. 14, no. 5, pp. 935–946, Oct. 2005.

[13] J. W. Tringe, T. A. Uhlman, A. C. Oliver, and J. E. Houston, "A single asperity study of Au/Au electrical contacts," *J. Appl. Phys.*, vol. 93, no. 8, pp. 4661–4669, 2003.

[14] Y. Chen, R. Nathanael, J. Jeon, J. Yaung, L. Hutin, and T.-J. K. Liu, "Characterization of contact resistance stability in MEM relays with tungsten electrodes," *J. Microelectromech. Syst.*, vol. 21, no. 3, pp. 511–513, Jun. 2012.

[15] J. A. Greenwood and J. B. P. Williamson, "Contact of nominally flat surfaces," *Proc. Roy. Soc. London A, Math. Phys. Eng. Sci.*, vol. 295, no. 1442, pp. 300–319, 1966.

[16] N. R. Tas, C. Gui, and M. Elwenspoek, "Static friction in elastic adhesion contacts in MEMS," *J. Adhes. Sci. Technol.*, vol. 17, no. 4, pp. 547–561, 2003.

[17] D. Maugis and H. M. Pollock, "Surface forces, deformation and adherence at metal microcontacts," *Acta Metall.*, vol. 32, no. 9, pp. 1323–1334, 1984.

[18] Y. Du, G. G. Adams, N. E. McGruer, and I. Etsion, "A parameter study of separation modes of adhering microcontacts," *J. Appl. Phys.*, vol. 103, no. 6, pp. 064902-1–064902-7, 2008.

[19] S. P. Bates, G. Kresse, and M. J. Gillan, "A systematic study of the surface energetics and structure of TiO_2(110) by first-principles calculations," *Surf. Sci.*, vol. 385, nos. 2–3, pp. 386–394, 1997.

[20] L. Vitos, A. V. Ruban, H. L. Skriver, and J. Kollár, "The surface energy of metals," *Surf. Sci.*, vol. 411, nos. 1–2, pp. 186–202, 1998.

[21] P. G. Slade, *Electrical Contacts: Principles and Applications*, 2nd ed. Boca Raton, FL, USA: CRC Press, 2013, pp. 1120–1198.

[22] H. L. Sun, Z. X. Song, D. G. Guo, F. Ma, and K. W. Xu, "Microstructure and mechanical properties of nanocrystalline tungsten thin films," *J. Mater. Sci. Technol.*, vol. 26, no. 1, pp. 87–92, 2010.

[23] H. Lee, R. A. Coutu, S. Mall, and K. D. Leedy, "Characterization of metal and metal alloy films as contact materials in MEMS switches," *J. Micromech. Microeng.*, vol. 16, no. 3, pp. 557–563, 2006.

[24] V. N. Sekhar, V. Srinivasarao, R. Jayaganthan, K. Mohankumar, and A. A. O. Tay, "A study on the mechanical behavior of the sputtered nickel thin films for UBM applications," in *Proc. 6th Electron. Packag. Technol. Conf.*, Dec. 2004, pp. 610–614.

[25] R. Timsit, "On the evalutation of contact temperature from potential-drop measurements," *IEEE Trans. Compon., Hybrids, Manuf. Technol.*, vol. 6, no. 1, pp. 115–121, Mar. 1983.

[26] G. L. Allen, R. A. Bayles, W. W. Gile, and W. A. Jesser, "Small particle melting of pure metals," *Thin Solid Films*, vol. 144, no. 2, pp. 297–308, 1986.

[27] G. H. Li *et al.*, "Measurement of adhesion forces between polycrystalline silicon surfaces via a MEMS double-clamped beam test structure," *J. Micromech. Microeng.*, vol. 20, no. 9, pp. 095015-1–095015-9, Sep. 2010.

Authors' photographs and biographies not available at the time of publication.